

Noise characterization for LISA

Julien Sylvestre* and Massimo Tinto†

Jet Propulsion Laboratory, California Institute of Technology, Pasadena, California 91109

(Dated: October 30, 2018)

We consider the general problem of estimating the inflight LISA noise power spectra and cross-spectra, which are needed for detecting and estimating the gravitational wave signals present in the LISA data. For the LISA baseline design and in the long wavelength limit, we bound the error on all spectrum estimators that rely on the use of the fully symmetric Sagnac combination (ζ). This procedure avoids biases in the estimation that would otherwise be introduced by the presence of a strong galactic background in the LISA data. We specialize our discussion to the detection and study of the galactic white dwarf-white dwarf binary stochastic signal.

PACS numbers: 04.80.Nn, 07.60.Ly, 95.55.Ym

I. INTRODUCTION

The LISA mission is a collaboration between ESA and NASA to build and operate a space-based laser interferometer aimed at detecting and studying gravitational waves (GW) of astrophysical origin. The current schedule places the launch around the year 2011, and the 3-10 years observation period is expected to produce a number of observations of galactic binaries [1], of massive black hole mergers and captures, and possibly of a cosmological stochastic background [2]. Early studies of the data analysis techniques that will be required to observe these signals are important since they couple our present knowledge about the sources LISA will be able to observe to the science requirements guiding the design of the LISA mission itself. It is in this context that we present here a study of the accuracy that can be expected for the characterization of the noise in the LISA detector once it has been placed in its heliocentric orbit. This is needed not only for being able to assess the LISA sensitivity in a region of the frequency band where the stochastic signal from coalescing galactic binaries would prevent it, but most importantly for being able to detect weak gravitational wave signals with confidence. Theoretical modeling and pre-launch performance measurements of flight-unit instruments will certainly be performed. However these might not be sufficient to achieve the level of accuracy required in the analysis of the data collected during the inflight operation of LISA.

Specifically, we calculate in the low frequency regime the optimal approximations for the spectra of the noise affecting the interferometric combinations sensitive to gravitational waves, by relying *only* on all the possible cross-spectra between the interferometric combinations that are sensitive to gravitational radiation and the symmetrized-Sagnac combination, ζ . The rationale behind this is that ζ couples very weakly to gravitational radiation while it is affected by the same instrumental noises as the other combinations [11]. These approximations give a lower bound on the error that can be achieved by estimators which make no prior assumptions about the characteristics of the various noise sources. Such estimator could be used for carrying out the full analysis, or for validating the noise models one could adopt for implementing more sophisticated and efficient data analysis techniques. An outline of the paper is given here.

Section II presents a review of the LISA baseline design, which is then followed by a discussion of the noise characterization problem in section III. In section IV we show that closure for the solution to the noise characterization problem does not exist, and that only approximate solutions can be implemented. In section V we describe the noise model used in our calculations, which accounts for possible cross-correlations between pairs of various noise sources. Although these terms have been neglected in the literature, they could contribute to the overall noise budget of the mission, and for this reason they are included in our analysis. We then present in section VI our calculation of the lower bound on the estimated noise spectra in the LISA interferometric combinations that are sensitive to gravitational radiation. In section VII we finally provide our comments on the implications of these bounds for the astrophysical reach of the LISA mission, and on possible implementations of noise estimation algorithms that would approach the error bounds we estimate.

*Electronic address: jsylvest@ligo.caltech.edu

†Electronic address: Massimo.Tinto@jpl.nasa.gov

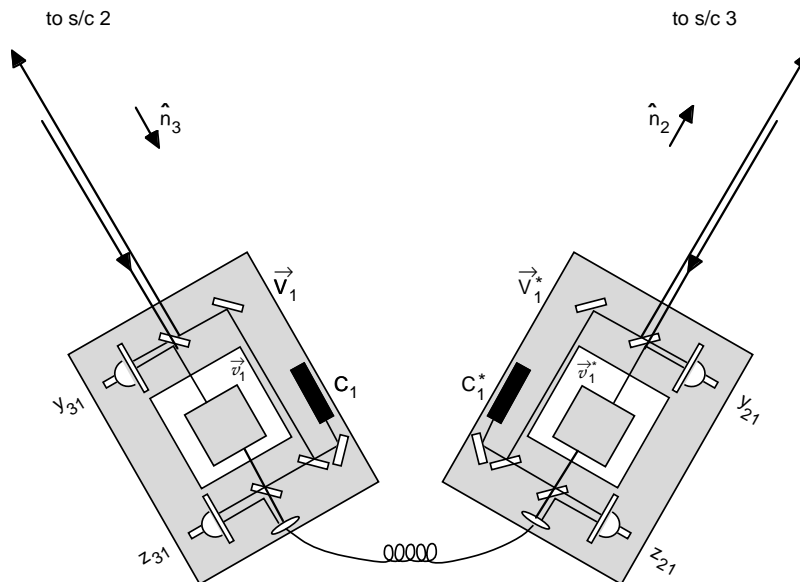


FIG. 1: Schematic description of the optical benches on spacecraft 1 in the LISA baseline design. Variables on the right hand bench are distinguished from corresponding variable from the left hand bench by asterisks. The measured Doppler signals are y_{31} and y_{21} . \hat{n}_i denote normal vectors along the triangle arms, and v_1 denotes the random velocity vector of proof mass 1.

II. LISA BASELINE DESIGN AND NOTATION

The LISA mission will consist of three spacecraft flying in an approximately equilateral triangle formation. The length of the arm opposite to spacecraft i ($i = 1, 2, 3$) is labeled L_i . The three nominal arm lengths will be equal to 16.7 s ($c = 1$), and they will differ from each other by at most a few percents during the entire duration of the mission. In contexts where the differences between the length of the arms can be disregarded, we will simply refer to the nominal arm length L , without indices. As it is illustrated in figure 1, each spacecraft will contain two optical benches. Each bench will be designed to bounce a laser beam between each of its proof mass and another proof mass on a distant spacecraft. The proof masses are mechanically isolated from their optical bench, and their relative position is measured with electrostatic sensors. These generate inputs for the drag-free control systems that allow the spacecraft to isolate the proof masses from external disturbances in such a way to maintain them (to a very good approximation) in a free-falling configuration in the directions to the other two spacecraft. In addition, laser beams will be bounced off the back of the proof masses and will be exchanged between the optical benches on a given spacecraft in order to sense the motion of the optical benches relative to the proof masses.

With this baseline design of the LISA spacecraft, the frequency noise of the lasers will dominate the secondary noise sources (such as acceleration noise of the proof masses or optical path length distortions) by approximately seven orders of magnitude in the frequency band of interest ($10^{-4} - 1$ Hz). Time delay interferometry (TDI) has been proposed [3, 4, 5] as a robust way for suppressing the frequency fluctuations from the lasers and the mechanical vibrations of the optical benches to levels smaller than that identified by the secondary noise sources. This is done by properly time-shifting and linearly combining the measurements of the phase differences between the coherent laser beams exchanged between the three pairs of spacecraft and the three pairs of on-board optical benches [5]. In reference [4] it has been shown that the entire space of the TDI combinations can be generated by four combinations, called α, β, γ and ζ , which are the Sagnac Interferometric combinations LISA will be able to synthesize. Since $(\alpha, \beta, \gamma, \zeta)$ can be regarded as a basis for the entire space of the LISA TDI combinations, in what follows we will limit our analysis to these four interferometric data.

It should be noted that the modifications of the Sagnac observable $(\alpha, \beta, \gamma, \zeta)$ required in order to account for the rotation of the LISA array [6] and variation in time of its arm lengths [7] can be disregarded in the analysis presented here. Although it will be critical to account for these effects in order to suppress the laser phase fluctuations below the secondary noise sources, the modifications introduced to the gravitational wave and secondary noise responses entering into the TDI combinations α, β, γ and ζ (derived under the assumption of a stationary LISA configuration) will be negligibly small.

It is anticipated that the dominant noises affecting all the TDI combinations will be introduced by the proof

masses and optical path noises (shot noise and beam pointing fluctuations). In the notation of Fig. 1, the frequency fluctuations generated by the mechanical vibrations of the proof masses are given by [5]

$$\begin{aligned}\zeta^{\text{proof mass}} &= \hat{\mathbf{n}}_1 \cdot (\mathbf{v}_{2,2} - \mathbf{v}_{2,13} + \mathbf{v}_{3,3}^* - \mathbf{v}_{3,21}^*) \\ &\quad + \hat{\mathbf{n}}_2 \cdot (\mathbf{v}_{3,3} - \mathbf{v}_{3,21} + \mathbf{v}_{1,1}^* - \mathbf{v}_{1,23}^*) \\ &\quad + \hat{\mathbf{n}}_3 \cdot (\mathbf{v}_{1,1} - \mathbf{v}_{1,23} + \mathbf{v}_{2,2}^* - \mathbf{v}_{2,13}^*),\end{aligned}\quad (1)$$

where bold characters are either vectors or matrices, $\mathbf{v}_{i,j} = \mathbf{v}_i(t - L_j)$, and $\mathbf{v}_{i,jk} = \mathbf{v}_i(t - L_j - L_k)$. We shall use below the definitions $v_1 = \hat{\mathbf{n}}_3 \cdot \mathbf{v}_3$, etc. Denoting by n_{ij} the optical path noise affecting the Doppler measurement y_{ij} , the optical path noise contribution to ζ is given by the following expression [5]

$$\zeta^{\text{optical path}} = n_{32,2} - n_{23,3} + n_{13,3} - n_{31,1} + n_{21,1} - n_{12,2}. \quad (2)$$

If we denote by ζ^{GW} the contribution to the ζ observable from a gravitational wave [5, Eq. (60)], it follows that ζ can be written in the following form

$$\zeta = \zeta^{\text{GW}} + \zeta^{\text{ins}}, \quad (3)$$

where the instrumental noise part is given instead by

$$\zeta^{\text{ins}} = \zeta^{\text{proof mass}} + \zeta^{\text{optical path}}. \quad (4)$$

In what follows we will be interested in calculating the spectrum of the ζ combination

$$S_{\zeta\zeta} = E[\tilde{\zeta}\tilde{\zeta}^*], \quad (5)$$

where $\tilde{\zeta}$ is the Fourier transform of ζ , and E denotes the expectation value over many realizations of the instrumental noise. In the particular case of a stochastic gravitational wave signal, the expectation value will be performed over the realizations of the signal too, although it always will be assumed to be independent of (and therefore uncorrelated with) the noise. Under these assumptions we can write

$$S_{\zeta\zeta} = S_{\zeta^{\text{GW}}\zeta^{\text{GW}}} + S_{\zeta^{\text{ins}}\zeta^{\text{ins}}}. \quad (6)$$

In what follows, for any pair of interferometric observables (x, y) , S_{xy} will refer to the following function of the Fourier frequency f

$$S_{xy} = S_{yx}^* = E[\tilde{x}\tilde{y}^*]. \quad (7)$$

For simplicity of notation we will write S_{xy}^{GW} for $S_{x^{\text{GW}}y^{\text{GW}}}$ and S_{xy}^{ins} for $S_{x^{\text{ins}}y^{\text{ins}}}$. As implied by Eqs.(1,2), the spectrum $S_{\zeta\zeta}^{\text{ins}}$ can be expanded in terms of proof mass and optical path noises as follows

$$\begin{aligned}S_{\zeta\zeta}^{\text{ins}} &= 4 \sin^2 \left(\frac{\omega L}{2} \right) \sum_{i=1}^3 [S_{v_i v_i} + S_{v_i^* v_i^*} + 2 \text{Re } S_{v_i v_i^*}] + \sum_{i=1}^2 \sum_{j=i+1}^3 [S_{n_{ij} n_{ij}} + S_{n_{ji} n_{ji}}] \\ &\quad - 2 \text{Re } [S_{n_{12} n_{13}} + S_{n_{21} n_{23}} + S_{n_{31} n_{32}}],\end{aligned}\quad (8)$$

where $\text{Re } x$ denotes the real part of x ($\text{Im } x$ is the imaginary part), and where for the sake of generality we have included terms accounting for correlations between proof masses on-board the same spacecraft and between optical path noises along the same arm (see section V for the physical motivations behind the inclusion of these correlations in our analysis).

III. IN-FLIGHT NOISE CHARACTERIZATION

As it is well known, the optimal statistics to detect a signal s in noisy data is the matched or Wiener filter, at least when the noise distribution can be well approximated as Gaussian. For the combination α , for instance, this statistics is

$$\int df \frac{\tilde{\alpha} \tilde{s}_\alpha^*}{S_{\alpha\alpha}}, \quad (9)$$

where s_α is the signal s filtered by the transfer function of gravitational wave to the combination α . As shown in [9], the three TDI Sagnac observables α , β , and γ can be combined to form the new data set A , E , and T . The advantage of these three combinations is in their noises being statistically uncorrelated for every frequency f ,

$$E[\tilde{A}\tilde{E}^*] = 0, \quad (10)$$

and similarly for all possible pairs taken among A , E , and T . The uncorrelated combinations are obtained by diagonalizing the correlation matrix

$$\mathbf{C} = \begin{pmatrix} S_{\alpha\alpha} & S_{\alpha\beta} & S_{\alpha\gamma} \\ S_{\alpha\beta}^* & S_{\beta\beta} & S_{\beta\gamma} \\ S_{\alpha\gamma}^* & S_{\beta\gamma}^* & S_{\gamma\gamma} \end{pmatrix}, \quad (11)$$

leading to an optimal detection statistics for the signal s that is given by

$$\int df \tilde{\mathbf{x}} \mathbf{C}^{-1} \tilde{\mathbf{x}}^\dagger, \quad (12)$$

where $\mathbf{x} = [\alpha, \beta, \gamma]$ and $\boldsymbol{\chi} = [s_\alpha, s_\beta, s_\gamma]$, for s_α , s_β , and s_γ the signal s filtered by the transfer functions of gravitational waves to the combinations α , β , and γ respectively. Eq. (9) is only a special case of Eq. (12), with \mathbf{C} , \mathbf{x} and $\boldsymbol{\chi}$ restricted to the one-dimensional case.

The optimal signal-to-noise ratio ρ_0 that can be achieved by Eq. (12) is [9]

$$\rho_0^2 = \int df \tilde{\boldsymbol{\chi}} \mathbf{C}^{-1} \tilde{\boldsymbol{\chi}}^\dagger. \quad (13)$$

Any variation of the detection statistics (up to a scaling factor) will give a smaller signal-to-noise ratio, so Eq. (12) is the optimal detection statistics. It is also true that the detection statistics of Eq. (12) maximizes the probability of detecting the signal for a fixed value of the false alarm probability.

Since the correlation matrix can only be known with some finite accuracy, we can write it in the following way

$$\mathbf{C} = \mathbf{C}_0 + \mathbf{C}_1, \quad (14)$$

where \mathbf{C}_0 is the true correlation matrix, and \mathbf{C}_1 is the error in its determination. By definition, the matrices \mathbf{C} , \mathbf{C}_0 and \mathbf{C}_1 must all be hermitian and positive definite. When the correlation matrix is measured with some error, the detection statistics of Eq. (12) constructed with the measured matrix is no longer optimal with respect to the true correlation matrix, and the SNR can be expected to be reduced. We present in Appendix A a derivation of the SNR loss due to the presence of the error \mathbf{C}_1 . To give an example of the magnitude of this effect, we can assume the estimate of the correlation matrix to have a given relative error, $(\mathbf{C}_1)_{ij} = \epsilon(\mathbf{C}_0)_{ij}$. Considering a fairly general signal [cf. Eq.(A6)], the relative SNR loss is then $\sim \epsilon/2$. These considerations indicate that in order to limit the SNR reduction to a negligible level (say $\sim 0.1\%$), the relative error on the measured spectra and cross-spectra for the three TDI combinations α , β , and γ should be of order 10% at most.

Errors in the determination of the spectra of the TDI combinations will also have an effect on the measurement of the parameters of the observed gravitational wave signals. Let $\mathbf{I}(\boldsymbol{\lambda})$ be the Fisher information matrix for the estimation of the parameters $\boldsymbol{\lambda}$ using data \mathbf{x} with distribution function $p(\mathbf{x}; \boldsymbol{\lambda})$:

$$\mathbf{I}(\boldsymbol{\lambda}) = -E \left[\frac{\partial^2 \log p(\mathbf{x}; \boldsymbol{\lambda})}{\partial \boldsymbol{\lambda}^2} \right]. \quad (15)$$

The Cramér-Rao bound gives a limit on the error cov $\hat{\boldsymbol{\lambda}}$ of an unbiased estimator $\hat{\boldsymbol{\lambda}}(\mathbf{x})$:

$$\text{cov } \hat{\boldsymbol{\lambda}} = E[(\hat{\boldsymbol{\lambda}}(\mathbf{x}) - \boldsymbol{\lambda})^\dagger (\hat{\boldsymbol{\lambda}}(\mathbf{x}) - \boldsymbol{\lambda})] \geq \mathbf{I}^{-1}(\boldsymbol{\lambda}). \quad (16)$$

As usual, the \geq sign in Eq.(16) means that the left hand side of the inequality minus its right hand side is positive semi-definite. An unbiased estimator can achieve the Cramér-Rao bound if and only if it has the form

$$\hat{\boldsymbol{\lambda}}(\mathbf{x}) = \boldsymbol{\lambda} + \left[\frac{\partial \log p(\mathbf{x}; \boldsymbol{\lambda})}{\partial \boldsymbol{\lambda}} \right]^T \mathbf{I}^{-1}(\boldsymbol{\lambda}). \quad (17)$$

Specializing to the case relevant here, where $\mathbf{x} = [\alpha, \beta, \gamma]$ and where $\boldsymbol{\chi}(\boldsymbol{\lambda}) = [s_\alpha(\boldsymbol{\lambda}), s_\beta(\boldsymbol{\lambda}), s_\gamma(\boldsymbol{\lambda})]$, assuming Gaussian noise, and going to the Fourier domain, one can write Eq.(17) into the following form after some simple algebra

$$\hat{\boldsymbol{\lambda}}(\tilde{\mathbf{x}}) = \boldsymbol{\lambda} + \text{Re} \left[\frac{\partial \tilde{\boldsymbol{\chi}}}{\partial \boldsymbol{\lambda}} \mathbf{C}^{-1} (\tilde{\mathbf{x}} - \tilde{\boldsymbol{\chi}})^\dagger \right]^T \mathbf{I}^{-1}, \quad (18)$$

where

$$\mathbf{I} = \frac{\partial \tilde{\chi}}{\partial \boldsymbol{\lambda}} \mathbf{C}^{-1} \frac{\partial \tilde{\chi}^\dagger}{\partial \boldsymbol{\lambda}}. \quad (19)$$

This estimator achieves the Cramér-Rao bound only if the right-hand side of Eq.(18) is independent of $\boldsymbol{\lambda}$, as the notation suggests; if this is not the case, no unbiased estimator can achieve the Cramér-Rao bound. For the analysis of data from LISA, one will use the estimator in Eq.(18), with some estimated value of \mathbf{C} that contains an error, as in Eq.(14). This estimator will necessarily have larger errors than the Cramér-Rao bound. Because the second term of the right-hand side of Eq.(18) is linear in $\tilde{\mathbf{x}} - \tilde{\chi}$, $\hat{\boldsymbol{\lambda}}(\tilde{\mathbf{x}})$ will be unbiased, independently of the size of the error \mathbf{C}_1 . It is shown in Appendix A that the error term in the covariance of the estimator constructed with the perturbed correlation matrix will vanish to first order in the perturbation \mathbf{C}_1 , so that, like the SNR, the variance of the estimated quantities will be at most second order in the measurement errors of the correlation matrix.

At high frequencies ($f \gtrsim 1$ mHz, [10]), the gravitational wave sources are expected to be discrete in time or in frequency, so that it should be possible to identify portions of the time series that are free of signal, and can therefore be used to estimate the spectra with an excellent accuracy (which is limited only by the integration time, and indirectly by the stationarity of the noise). At lower frequencies, on the other hand, gravitational waves from the galactic binaries will not be distinguishable, and will form a stochastic signal above the instrumental noise. Strong signals that are above this confusion limit might be detected and analyzed with respect to the noise from the binaries, which can be estimated with high accuracy by integrating the data for a long enough time. The most direct application of the characterization of the noise at low frequencies is thus the measurement of the stochastic background itself. In other words, it is highly desirable to have techniques that can effectively “turn off” the gravitational signal, in order to properly characterize the instrumental noise. At higher frequencies, these techniques should not be crucial for the detection of weak signals, but should be very useful in understanding and validating the detector performance. To give a specific example, it might be useful at some point to verify that a given spectral line is of astrophysical origin and is not instrumental, without having to rely on astrophysical assumptions (such as the Doppler modulation of the signal).

In the simplest search, a stochastic background will be detected by comparing the measured spectra $S_{\alpha\alpha}$, $S_{\beta\beta}$, and $S_{\gamma\gamma}$ to the estimate of the instrumental noise. Differences between the measured and the estimated spectra will be interpreted as a stochastic background. It therefore goes without saying that the low frequency portion of the instrumental noise spectra in those TDI combinations must be estimated as well as possible.

As it has been recognized in [11], the TDI combination ζ (i.e., the fully symmetric Sagnac combination) is much less sensitive to gravitational waves than the other Sagnac combinations (α, β, γ) in the low part of the frequency band accessible to LISA ($f \lesssim 30$ mHz), although it is affected by the same instrumental noise sources. Consequently, it can be used as a “gravitational waves shield” to estimate the instrumental noise. This approach was introduced by [11] to bound the power in the stochastic background. Since the GW signal is additive in the noise of the TDI combinations,

$$S_{XX} = S_{XX}^{\text{ins}} + S_{XX}^{\text{GW}}, \quad (20)$$

where S_{XX} is the measured spectrum of the Unequal-Arm Michelson combination X , S_{XX}^{ins} is the spectrum of the instrumental noise in X , and S_{XX}^{GW} is the spectrum of a stochastic background. It is shown in [11] that the following inequality holds

$$S_{XX}^{\text{GW}} \geq S_{XX} - \hat{S}_{XX}^{\text{ins}}, \quad (21)$$

where the *upper bound* on the instrumental noise spectrum is, in the low-frequency region of the LISA band,

$$\hat{S}_{XX}^{\text{ins}} = 16S_{\zeta\zeta}^{\text{ins}} - 128\pi^2 f^2 L^2 V - 32(3 - 4\pi^2 f^2 L^2)N, \quad (22)$$

with V being a lower bound on the spectrum of the acceleration noise of all proof masses, and N a lower bound on the spectrum of the optical noise of all optical paths.

A somewhat similar approach is used in [12] to estimate the *average* of three TDI combinations, $\bar{S} = (S_{XX} + S_{YY} + S_{ZZ})/3$. They estimate \bar{S}^{ins} by multiplying $S_{\zeta\zeta}$ by a judiciously chosen transfer function, and subtract the result from the measured \bar{S} to get \bar{S}^{GW} . This “averaged” estimator is quite different from what we will consider below, and will not be discussed further.

IV. MODEL INDEPENDENT APPROACH

At low frequencies, the real function $S_{\zeta\zeta}$ and the three complex functions $S_{\alpha\zeta}$, $S_{\beta\zeta}$, and $S_{\gamma\zeta}$, give seven measurements that are insensitive to gravitational waves, in the sense that $S_{\theta\zeta} \simeq S_{\theta\zeta}^{\text{ins}}$, $\theta = \alpha, \beta, \gamma, \zeta$. Since the four TDI generators

fulfill the following identity

$$\begin{aligned}
[1 - e^{i\omega(L_1+L_2+L_3)}]\tilde{\zeta} = & \left[e^{i\omega L_1} - e^{i\omega(L_2+L_3)} \right] \tilde{\alpha} + \\
& \left[e^{i\omega L_2} - e^{i\omega(L_1+L_3)} \right] \tilde{\beta} + \\
& \left[e^{i\omega L_3} - e^{i\omega(L_1+L_2)} \right] \tilde{\gamma},
\end{aligned} \tag{23}$$

the seven functions introduced above are not all independent. In particular, we could try to estimate $S_{\alpha\alpha}^{\text{ins}}$ by a linear combination of the cross-spectra $S_{\alpha\zeta}$, $S_{\beta\zeta}$, $S_{\gamma\zeta}$, and $S_{\zeta\zeta}$ as

$$S_{\alpha\alpha}^{\text{ins}} = aS_{\alpha\zeta} + bS_{\beta\zeta} + cS_{\gamma\zeta} + zS_{\zeta\zeta}. \tag{24}$$

Using the identity Eq.(23) to expand the right-hand side of Eq.(24) and collecting terms in $S_{\alpha\alpha}^{\text{ins}}$ gives

$$[\cos\omega L_1 - \cos\omega(L_2 + L_3)]a + [1 - \cos\omega(L_1 - L_2 - L_3)]z = 1 - \cos\omega(L_1 + L_2 + L_3). \tag{25}$$

Further requiring all the other terms in the right-hand side of Eq.(24) to be zero gives eight other equations. However, the only solution satisfying those eight equations is

$$\begin{aligned}
(a, b, c, z) = & (\cos\omega(L_1 - L_2) - \cos\omega L_3, 1 - \cos\omega(L_1 - L_2 + L_3), \\
& -\cos\omega L_1 + \cos\omega(L_2 - L_3), \frac{[\cos\omega(L_1 + L_2 + L_3) - 1] \sin \frac{\omega}{2}(L_1 - L_2 + L_3)}{\sin \frac{\omega}{2}(L_1 + L_2 + L_3)})
\end{aligned} \tag{26}$$

and this solution does not satisfy Eq.(25). This implies that $S_{\alpha\alpha}^{\text{ins}}$ cannot be reconstructed from measurements of spectra that are insensitive to gravitational waves. The argument can be extended to other spectra with β and γ . It is therefore necessary to consider combinations of the insensitive spectra that are only approximations to the spectra involving α , β , and γ .

V. NOISE MODEL

In what follows we first define a realistic noise model for LISA. The best combination of the spectra and cross-spectra involving ζ for this model will be derived in the next section, where it will be used to set a bound on the accuracy that can be achieved in characterizing the LISA noise spectra

The principal source of noise at low frequencies is the acceleration noise of the proof masses along their sensitive axes. A number of effects lead to acceleration noises which sum up to a noise budget (per proof mass) of 3×10^{-15} m s⁻² Hz^{-1/2} at 0.1 mHz [13]. The principal sources of acceleration noise might be due to [14]: thermal distortion of the spacecraft, cross-talk between the other degrees of freedom and the sensitive axis, gravity gradient noise due to spacecraft displacements, fluctuating spacecraft magnetic fields, thermal noise, back-action from sensing, electric forces from fluctuating charge, residual gas, magnetic damping, temperature variations, etc. It should be noted that the first four noise sources might affect *both* proof masses on a given spacecraft, so that the acceleration noises of the two masses will be correlated to some extent. This might be important for the correct estimation of the noise level that will be achievable with TDI [15]. In this paper, we will assume that the acceleration noises, converted in terms of relative frequency fluctuations, are given by [5]

$$S_{v_i v_i} = S_{v_i^* v_i^*} = 2.5 \times 10^{-48} \left(\frac{1 \text{ Hz}}{f} \right)^2 \text{ Hz}^{-1} \tag{27}$$

$$S_{v_i v_j^*} = \xi S_{v_i v_i} \delta_{ij} \tag{28}$$

where $i, j = 1, 2, 3$, δ_{ij} is Kronecker's delta, and ξ is an arbitrary complex number with norm $|\xi| \leq 1$. The correlated noises should couple to the proof masses either gravitationally or magnetically, so the phase angle of ξ will only depend on the spatial distribution of the perturbing field with respect to the sensitive axes of the two proof masses.

At frequencies above ~ 5 mHz, the optical path noises dominate the total sensing noise. The optical path noise budget [13] includes contribution from the shot noise affecting the phase measurement at the photodiodes, as well as phase fluctuations resulting from scattered light effects, laser beam pointing instabilities, and path length variations on the benches and within the telescopes. The latter two effects will couple the optical path noise along various paths: pointing instabilities will correlate the noise along the paths related to benches i and i^* , while the path length

variations will mostly introduce correlations at times offset by the one-way-light-time L between the measurements from beams going in opposite direction along a given arm. In what follow we will make the assumption that the latter effect is dominating the cross-correlation of the optical path noise, and write the following expressions for the optical path noise spectra and cross-spectra

$$S_{n_{ij}n_{ij}} = 1.8 \times 10^{-37} \left(\frac{f}{1 \text{ Hz}} \right)^2 \text{ Hz}^{-1} \quad (29)$$

$$S_{n_{ij}n_{ik}} = -2\chi \cos(2\pi fL) S_{n_{ij}n_{ij}} \quad (30)$$

where $i, j, k = 1, 2, 3$, $i \neq j$, $i \neq k$, $j \neq k$, and χ is a positive real number. The cosine term in Eq.(30) comes from the time delay L for the propagation of phase noise along one of the LISA arms.

In what follows we will use two noise models. In the first case we will be optimistic and assume all cross-correlation terms to be negligible, i.e. we will pick $\xi = \chi = 0$. In the second, pessimistic case, significant correlations will be assumed to be present. For the acceleration noise, we take $|\xi| = 0.25$, corresponding to the fact that roughly 50% of the noise budget (in strain) corresponds to noise sources that can induce strong correlations between the two proof masses on-board one spacecraft. Since there is no specific reason for preferring a particular value of the phase for ξ over any other, we will treat it as a free parameter in our analysis. We will also pick $\chi = 0.05$, based on the fact that roughly 15% of the optical-path noise budget (in strain) is attributed to path length variations on the optical benches and the telescopes. It should obviously be noted that these noise models will probably not give a realistic description of the noise that will affect the LISA measurements. They are only chosen to provide some guidance in the noise characterization problem.

VI. ERROR BOUND ON THE ESTIMATED SPECTRA

In this section we calculate the smallest possible errors between the estimated and real instrumental spectra that can be achieved by using only the GW-free measurements $S_{\theta\zeta}$, where $\theta = \alpha, \beta, \gamma, \zeta$. These spectra are the only ones that are free of laser frequency noise and of GW signals, and therefore form a natural basis for building noise estimators that do not rely on unverifiable assumptions about the properties of the noise sources. Our error bounds will obviously depend on the noise model used, and so will the estimators that achieve these bounds that we will present. These estimators will therefore not be valid estimators for the characterization of the LISA noise; model independent estimators that approach our error bounds will be presented in a follow-up communication.

Each TDI combination will show a different transfer function for the noise contributions identified in the previous section. In particular, every spectrum will be a linear combination of the acceleration and optical noise spectra, so that any instrumental noise spectrum $S_{\mu\nu}^{\text{ins}}$ (μ, ν are any TDI combinations) can be written as

$$S_{\mu\nu}^{\text{ins}} = \mathbf{T}_{\mu\nu} \cdot \mathbf{S}_N, \quad (31)$$

where $\mathbf{T}_{\mu\nu}$ is a complex vector of frequency dependent coefficients, and \mathbf{S}_N is the real vector of the 21 noise spectra

$$\begin{aligned} \mathbf{S}_N = & (S_{v_1v_1}, S_{v_1^*v_1^*}, \text{Re } S_{v_1v_1^*}, \text{Im } S_{v_1v_1^*}, \\ & S_{v_2v_2}, S_{v_2^*v_2^*}, \text{Re } S_{v_2v_2^*}, \text{Im } S_{v_2v_2^*}, \\ & S_{v_3v_3}, S_{v_3^*v_3^*}, \text{Re } S_{v_3v_3^*}, \text{Im } S_{v_3v_3^*}, \\ & S_{n_{12}n_{12}}, S_{n_{13}n_{13}}, S_{n_{12}n_{13}}, \\ & S_{n_{21}n_{21}}, S_{n_{23}n_{23}}, S_{n_{21}n_{23}}, \\ & S_{n_{31}n_{31}}, S_{n_{32}n_{32}}, S_{n_{31}n_{32}}). \end{aligned} \quad (32)$$

The $S_{\theta\zeta}$ spectra only have terms of the form $S_{v_i v_i} + \text{Re } S_{v_i v_i^*}$, $S_{v_i^* v_i^*} + \text{Re } S_{v_i v_i^*}$, or $\text{Im } S_{v_i v_i^*}$. This is because ζ has the same transfer function to \mathbf{v}_i and to \mathbf{v}_i^* , so any spectrum $S_{\theta\zeta}$ will only have terms of the form $S_{v_i v_i} + S_{v_i^* v_i^*}$ and $S_{v_i v_i^*} + S_{v_i^* v_i^*}$. Consequently, only three of the four quantities $S_{v_i v_i}$, $S_{v_i^* v_i^*}$, $\text{Re } S_{v_i v_i^*}$ and $\text{Im } S_{v_i v_i^*}$ can be measured simultaneously. A similar argument applies for the optical noises. In that case, a $S_{\theta\zeta}$ spectrum measures the combinations $S_{n_{ij}n_{ij}} - S_{n_{ik}n_{ij}}^*$ and $S_{n_{ik}n_{ik}} - S_{n_{ik}n_{ij}}$, so one can only measure $S_{n_{ij}n_{ij}} - \text{Re } S_{n_{ik}n_{ij}}$, $S_{n_{ik}n_{ik}} - \text{Re } S_{n_{ik}n_{ij}}$, and $\text{Im } S_{n_{ik}n_{ij}}$ simultaneously. Inequalities in the lengths of the arms may break these symmetries.

The coefficient vector $\mathbf{T}_{\mu\zeta}$ is known from the definition of the TDI combinations, and it just consists of geometrical transfer functions. Clearly, there is not enough information to measure every one of the 21 terms in \mathbf{S}_N . This means that an approximated solution has to be used. Supposing we want to measure the instrumental spectrum $S_{\mu\nu}^{\text{ins}}$, we can measure $S_{\alpha\zeta}$, $S_{\beta\zeta}$, $S_{\gamma\zeta}$, and $S_{\zeta\zeta}$, and then approximate $\mathbf{T}_{\mu\nu}$ with the following expression

$$\hat{\mathbf{T}}_{\mu\nu} = a\mathbf{T}_{\alpha\zeta} + b\mathbf{T}_{\beta\zeta} + c\mathbf{T}_{\gamma\zeta} + z\mathbf{T}_{\zeta\zeta}. \quad (33)$$

The estimated spectrum $\hat{S}_{\mu\nu}^{\text{ins}}$ is then given by

$$\begin{aligned}\hat{S}_{\mu\nu}^{\text{ins}} &= \hat{\mathbf{T}}_{\mu\nu} \cdot \mathbf{S}_N \\ &= aS_{\alpha\zeta} + bS_{\beta\zeta} + cS_{\gamma\zeta} + zS_{\zeta\zeta}.\end{aligned}\tag{34}$$

Performing the approximation in Eq.(33) requires the definition of a proper error metric. In this paper, we choose a model dependent metric in order to bound the achievable error on the estimated spectrum. For complex $\mathbf{T}_{\mu\nu}$ vectors, we minimize the error on $\text{Re}[\mathbf{T}_{\mu\nu}]$ and $\text{Im}[\mathbf{T}_{\mu\nu}]$ independently. Specifically, we minimize the error $\|\text{Re}[\hat{\mathbf{T}}_{\mu\nu}] - \text{Re}[\mathbf{T}_{\mu\nu}]\|^2$ and $\|\text{Im}[\hat{\mathbf{T}}_{\mu\nu}] - \text{Im}[\mathbf{T}_{\mu\nu}]\|^2$, where $\text{Re}[\hat{\mathbf{T}}_{\mu\nu}]$ and $\text{Im}[\hat{\mathbf{T}}_{\mu\nu}]$ are restricted to the space spanned by the vectors $\text{Re}[\mathbf{T}_{\mu\zeta}]$ and $\text{Im}[\mathbf{T}_{\mu\zeta}]$ respectively, and where

$$\|\mathbf{x}\|^2 = (\mathbf{x}, \mathbf{x})\tag{36}$$

for the scalar product

$$(\mathbf{x}, \mathbf{y}) = \sum_{i=1}^{21} x_i (\mathbf{S}_N)_i^2 y_i.\tag{37}$$

This error norm penalizes error on individual noise components proportionally to their contribution to the spectrum $S_{\mu\nu}^{\text{ins}}$. The approximation casted in this form is a linear least-squares estimation problem, which can be solved easily using standard techniques. In particular, the vectors $\mathbf{T}_{\alpha\zeta}$, $\mathbf{T}_{\beta\zeta}$, $\mathbf{T}_{\gamma\zeta}$, and $\mathbf{T}_{\zeta\zeta}$ are not linearly independent, and therefore the solution $\hat{\mathbf{T}}_{\mu\nu}$ is not unique. We pick the solution with the smallest Euclidean norm, as in [16, Eq. (2.6.7)].

In order to explore the influence of correlations on the measurement of the spectra, we consider the two choices of ξ and χ defined in section V. For the case of no correlations, we show in figure 2 the overlaps

$$[S_{\alpha\alpha}^{\text{ins}}, S_{\theta\zeta}] = \frac{(S_{\alpha\alpha}^{\text{ins}}, S_{\theta\zeta})}{\sqrt{\|S_{\alpha\alpha}^{\text{ins}}\|^2 \|S_{\theta\zeta}\|^2}}.\tag{38}$$

Below ~ 2 mHz, none of the $S_{\theta\zeta}$ have very good overlap with $S_{\alpha\alpha}^{\text{ins}}$, but above that frequency, $S_{\alpha\alpha}^{\text{ins}}$ is very close to $S_{\zeta\zeta}$. We can thus expect a good least square fit for $f \gtrsim 3$ mHz, which is what Fig. 3 shows. The relative least square error is

$$\frac{\|\hat{\mathbf{T}}_{\alpha\alpha} - \mathbf{T}_{\alpha\alpha}\|}{\|\mathbf{T}_{\alpha\alpha}\|},\tag{39}$$

and the relative error e on the spectrum is

$$e = \frac{\hat{S}_{\alpha\alpha}^{\text{ins}} - S_{\alpha\alpha}^{\text{ins}}}{S_{\alpha\alpha}^{\text{ins}}}.\tag{40}$$

The spectrum error peaks at -24.5% at 0.76 mHz, although it is small in some low-frequency bands. The other non-trivial spectrum for $\xi = \chi = 0$ is $\text{Re } S_{\alpha\beta}^{\text{ins}}$. All cross-spectra are real, and spectra involving β and γ are identical to $S_{\alpha\alpha}^{\text{ins}}$ or $S_{\alpha\beta}^{\text{ins}}$. The overlaps are shown in Fig.4, while the relative errors are shown in Fig.5. Again, the overlaps are good for $f \gtrsim 1$ mHz, and the least square and spectrum errors are small. The spectrum $S_{\alpha\beta}^{\text{ins}}$, however, has a zero around 0.22 mHz, which cannot be fitted by the $S_{\theta\zeta}$ measurements. This leads to the large relative error on the spectrum below 1 mHz.

For the pessimistic case with $|\xi| = 0.25$ and $\chi = 0.05$, the characteristics of the approximation varies with the arguments of ξ . As argued in section V, a zero argument for χ is probably realistic. To get a specific example, we also fix the argument of ξ to be zero, and plot the results of the least square fit for $S_{\alpha\alpha}^{\text{ins}}$ in Fig. 6. It can be seen that at high frequencies the error is increased significantly by the small amount of correlation in the optical path noise. At low frequencies, correlations do not appear to significantly increase the error of the fit. Fig. 7 shows how the error varies with the phase angles of ξ , thus revealing the importance of the acceleration noise correlations. Depending on the argument of ξ , the estimation relative error can vary by as much as 10% at low frequencies.

In general, some cross-spectra might be complex, but for the noise model of section V, they will all be real, if the phase of ξ is zero. We present in Fig. 8 the results of the least square fit for $\text{Re } S_{\alpha\beta}^{\text{ins}}$, for the case $\xi = 0.25$ and $\chi = 0.05$. As it can clearly be seen, the correlations exacerbate the problem of fitting the zero near 0.22 mHz.

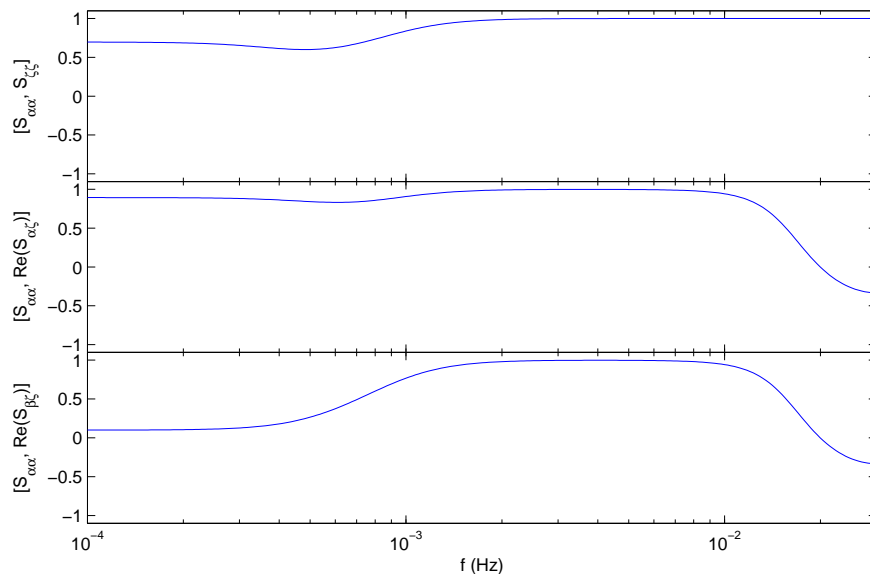


FIG. 2: Overlaps between the instrumental noise $S_{\alpha\alpha}^{\text{ins}}$ and the measured spectra $S_{i\zeta}$. By symmetry, the overlap $[S_{\alpha\alpha}^{\text{ins}}, \text{Re}(S_{\gamma\zeta})]$ is identical to the overlap $[S_{\alpha\alpha}^{\text{ins}}, \text{Re}(S_{\beta\zeta})]$ (third panel). Overlaps with the imaginary parts of the complex cross-spectra are all zero.

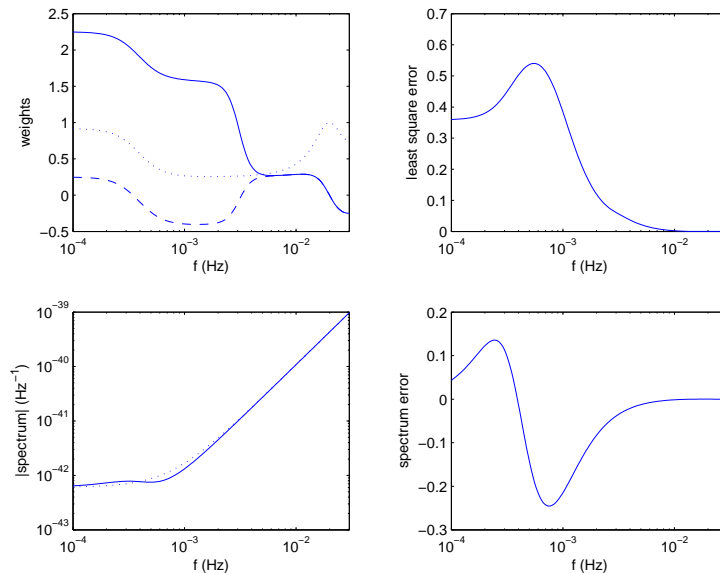


FIG. 3: Results of the least square fit of $S_{\alpha\alpha}^{\text{ins}}$. Top left: the weights a (continuous line), b (dashed line), c (dashed line), and z (dotted line). Top right: the normalized least square error. Bottom left: $S_{\alpha\alpha}^{\text{ins}}$ (dotted line) and $\hat{S}_{\alpha\alpha}^{\text{ins}}$ (continuous line). Bottom right: the normalized error on the estimated spectrum.

VII. DISCUSSION

We have presented an analysis of the prospects for a precise characterization of the noise of the LISA detector once it begins to operate as a gravitational wave detector. We have derived a set of bounds on the error of the spectra and cross-spectra of the TDI combinations that will be necessary for the analysis of the data. The most important feature of these bounds is that they are derived almost without any assumptions about the form of the individual noise sources. The only exception is that we assume certain cross-correlations to be negligible in order to keep a manageable number of terms; there are, however, no fundamental limitations to including additional terms in future

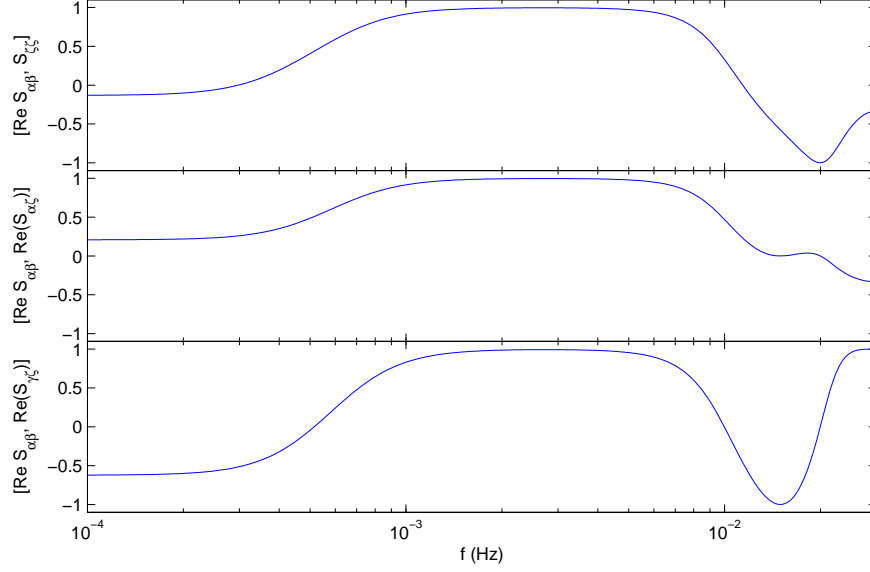


FIG. 4: Overlaps between the instrumental noise $\text{Re } S_{\alpha\beta}^{\text{ins}}$ and the measured spectra $S_{i\zeta}$. By symmetry, the overlap $[\text{Re } S_{\alpha\beta}^{\text{ins}}, \text{Re } S_{\beta\zeta}]$ is identical to the overlap $[\text{Re } S_{\alpha\beta}^{\text{ins}}, \text{Re } S_{\gamma\zeta}]$ (third panel).

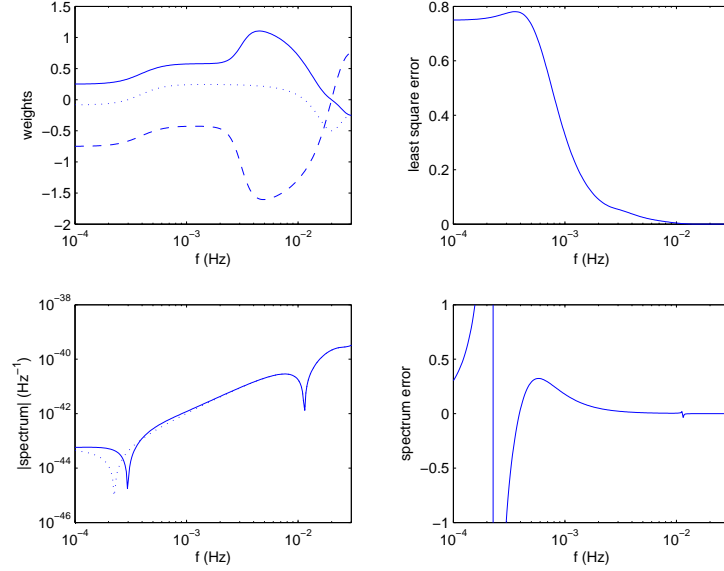


FIG. 5: Results of the least square fit of $\text{Re } S_{\alpha\beta}^{\text{ins}}$. Top left: the weights a (continuous line), b (continuous line), c (dashed line), and z (dotted line). Top right: the normalized least square error. Bottom left: $\text{Re } S_{\alpha\beta}^{\text{ins}}$ (dotted line) and $\text{Re } \hat{S}_{\alpha\beta}$ (continuous line). The dips in these curves are unresolved zeros. Bottom right: the normalized error on the estimated spectrum.

analyses. The bounds that we obtained simply reflect how well a given spectrum can be approximated by a linear combination of spectra that are insensitive to gravitational waves, and therefore only sample the instrumental noise.

Our error bounds are different from those given in [11] and [12], which assumed pre-launch measurements or estimates of the acceleration and optical path noises to be available in constructing their estimators of the spectra. In contrast, we have calculated the optimal error bound that can be achieved by an estimator that does not use prior assumptions about the spectra of the various noises. These bounds will be most useful for the development of model-independent estimators, which will be the subject of a follow-up paper. It is important to emphasize that model-independent estimators will be critical for the unambiguous detection and study of GW sources with LISA,

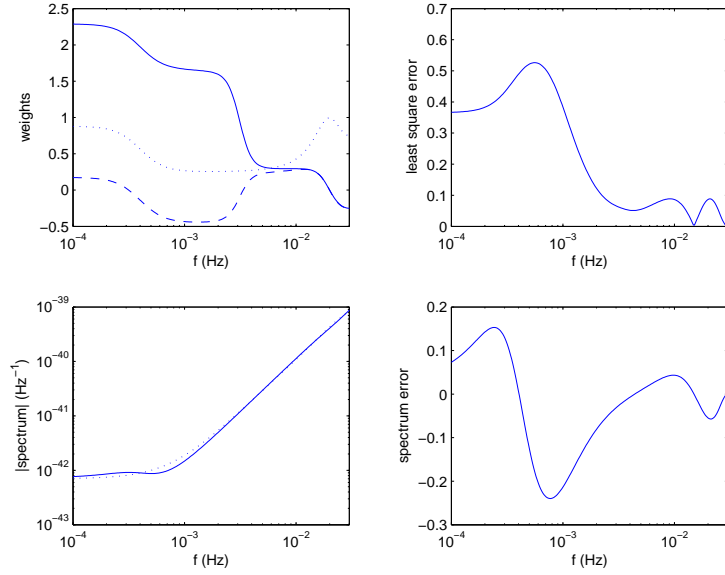


FIG. 6: Same as Fig.3 for $\xi = 0.25$ and $\chi = 0.05$.

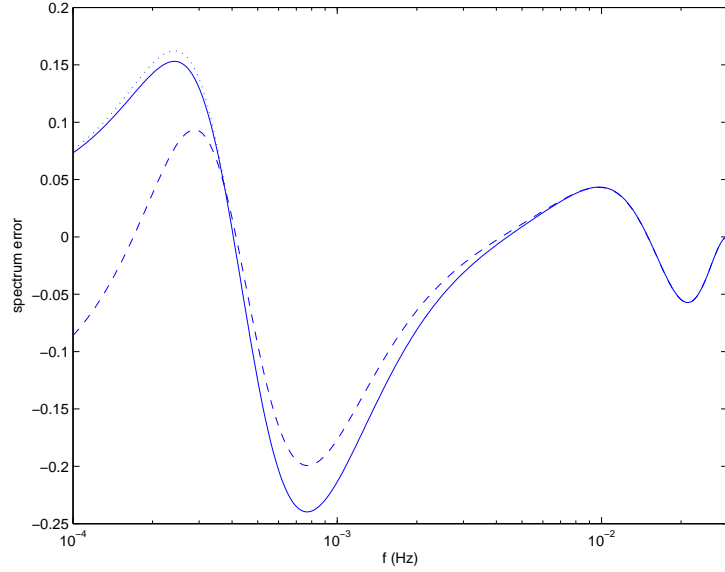


FIG. 7: Normalized error on the estimated spectrum, for different values of the arguments of ξ . The continuous line is for $\arg \xi = 0$, and the dashed line is for $\arg \xi = \pi$. These two curves bound the variation of the error at all frequencies above 0.39 mHz. Below 0.39 mHz, a larger error (dotted line) is possible for a complex ξ .

and possibly for the validation of the instrument and of other model-dependent estimators.

To give a specific example, we plot in Fig. 9 our best-fitted spectrum and the estimated spectrum from [11] for the S_{XX}^{ins} spectrum, assuming no correlations ($\chi = \xi = 0$). As shown in Eq. (22), the spectrum estimator from [11] requires a knowledge of how small the acceleration and optical path noises can be. Without reliable prior information, the lower limit can only be assumed to be zero, and the spectrum estimate is $\hat{S}_{XX}^{\text{ins}} = 16S_{\zeta\zeta}$, which is considerably worse than the least-square spectrum. One has to be able to guarantee that the noise is at least larger than 90% of the design value so that the spectrum estimate performs as well as the optimal least square estimator.

If the real stochastic background is as strong as the one plotted in Fig. 9, it will be detectable unambiguously by just comparing the measured spectrum S_{XX} to sixteen times the measured spectrum $S_{\zeta\zeta}$. However, the measurement of the excess power at each frequency of S_{XX} will carry a systematic error from the imperfect characterization of

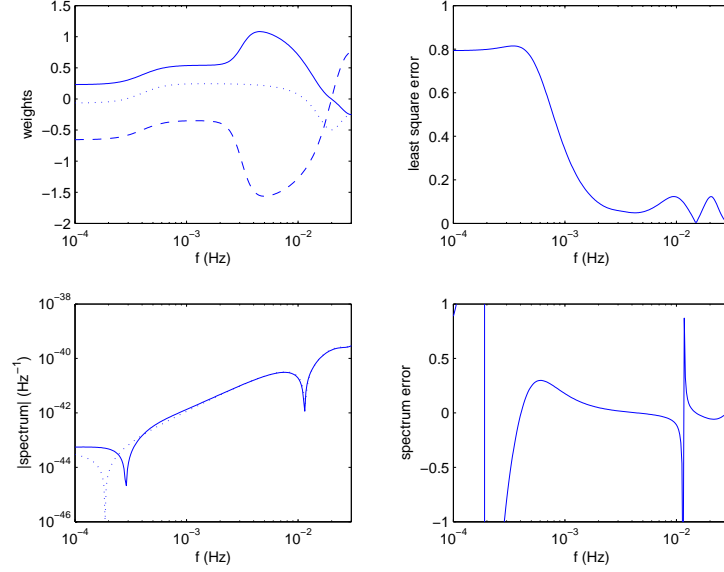


FIG. 8: Same as Fig. 5 for $\xi = 0.25$ and $\chi = 0.05$.

the noise. In the model that we considered above, this error would bring down the largest frequency at which the background can be reliably estimated from ~ 2 mHz to ~ 1 mHz.

To conclude, our bounds show that the spectra relevant to LISA's data analysis can only be measured to relative errors of the order of 10% if the estimation is restricted to using only the model-independent, signal-independent quantities $S_{\theta\zeta}$, for $\theta = \alpha, \beta, \gamma, \zeta$. It should be possible to unambiguously detect large stochastic backgrounds, by comparing S_{XX} to $16S_{\zeta\zeta}$, for instance. Uncertainties in the characterization of LISA's noise will principally introduce errors in the estimation of the power spectrum of the stochastic background.

Acknowledgments

This research was performed by the Jet Propulsion Laboratory, California Institute of Technology, under contract with the National Aeronautics and Space Administration.

APPENDIX A: SNR LOSS AND DEGRADATION IN PARAMETER ACCURACY

We present in this appendix a derivation of the formulae describing the degradation of the SNR and of the error on the estimated parameters of a GW signal due to errors in the estimation of the spectra and cross-spectra describing the noise in the LISA detector. For matched filtering, the detection statistics is given by

$$\Lambda = \int df \mathbf{x} \mathbf{C}^{-1} \boldsymbol{\chi}^\dagger. \quad (\text{A1})$$

The SNR ρ for this statistics can easily be shown to be

$$\rho^2 = \frac{(\int df \boldsymbol{\chi} \mathbf{C}^{-1} \boldsymbol{\chi}^\dagger)^2}{\int df \boldsymbol{\chi} \mathbf{C}^{-1} \mathbf{C}_0 \mathbf{C}^{-1} \boldsymbol{\chi}^\dagger}, \quad (\text{A2})$$

where the correlation matrix is assumed to contain an error as described by Eq. (14). When the correlation matrix is perfectly known ($\mathbf{C}_1 = 0$), Eq.(A2) reduces to Eq.(13). The \mathbf{C}_0 matrix in the denominator of Eq.(A2) comes from the expectation of $|\Lambda|^2$ when only the instrumental noise is present.

If $\mathbf{C}_1 \ll \mathbf{C}_0$, the Neumann expansion can be used to write

$$\mathbf{C}^{-1} = \mathbf{C}_0^{-1} - \mathbf{C}_0^{-1} \mathbf{C}_1 \mathbf{C}_0^{-1} + \mathbf{C}_0^{-1} \mathbf{C}_1 \mathbf{C}_0^{-1} \mathbf{C}_1 \mathbf{C}_0^{-1} + O(\mathbf{C}_1^3). \quad (\text{A3})$$

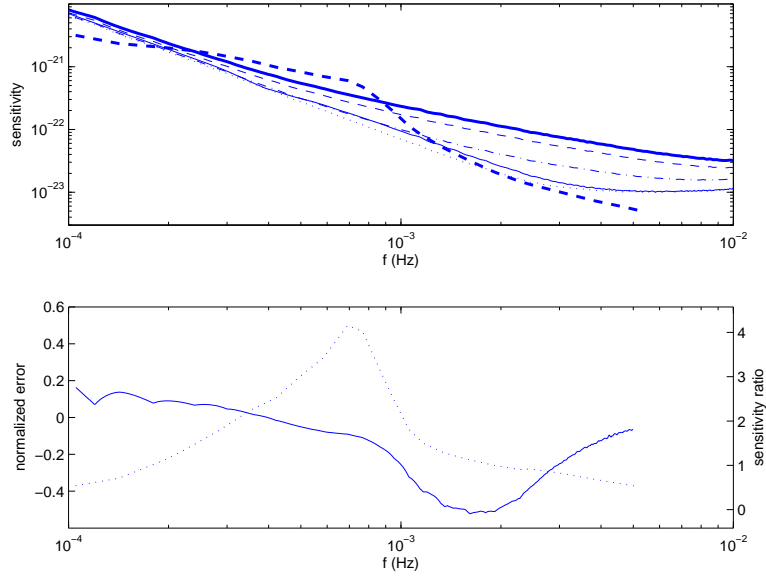


FIG. 9: *Top*: a comparison of our least square bound (thin continuous line) with the bound of [11, Eq. (12)] (dash-dotted line for a lower bound on V and N (S^0 and S^1 in the notation of [11]) of 90% of their design values, and the thin dashed line for a lower bound of 50% of their design values), for the sensitivity of S_{XX}^{ins} (dotted line) with $\xi = \chi = 0$, for 1 year of observation and a signal to noise ratio of 5 (the sensitivity is averaged over sky position and polarization angle, as in [5]). The thick continuous line shows the sensitivity for $16S_{\zeta\zeta}$, the limit of the method of [11] when V and N are allowed to be vanishingly small. The thick dashed line shows the confusion noise from binaries calculated by [17] (dashed line in their Fig. 2). *Bottom*: the normalized systematic error on the sensitivity of X (continuous line, left axis), computed from the least square bound minus the sensitivity of S_{XX}^{ins} , divided by the strain in the stochastic background, and the ratio of the sensitivity of S_{XX}^{ins} to the strain in the stochastic background (dotted line, right axis).

Expanding Eq.(A2) in the small matrix \mathbf{C}_1 , straightforward but lengthy algebra shows that the first order terms vanish, and that

$$\rho^2 = \rho_0^2 \left[1 - \frac{1}{\rho_0^2} \int df \chi \mathbf{C}_0^{-1} \mathbf{C}_1 \mathbf{C}_0^{-1} \mathbf{C}_1 \mathbf{C}_0^{-1} \chi^\dagger + \frac{1}{\rho_0^4} \left(\int df \mathbf{C}_0^{-1} \mathbf{C}_1 \mathbf{C}_0^{-1} \chi^\dagger \right)^2 \right], \quad (\text{A4})$$

where ρ_0 is the SNR achievable when $\mathbf{C}_1 = 0$.

If \mathbf{C} is known up to a scale factor for all frequencies where the signal is present, for instance, then Eq.(A4) shows as expected that the SNR is unaffected. If, however, the error on \mathbf{C} is frequency dependent over the frequency range where the signal contributes significantly to the SNR, the filter used to construct Λ will be far from optimal, and significant degradation in the SNR will occur. Supposing for simplicity that the signal contributes uniformly to the SNR over a bandwidth B , and supposing that the error on the correlation matrix is $\mathbf{C}_1 = \epsilon \mathbf{C}_0$ over a bandwidth b included in the signal frequency range, then

$$\rho^2 \simeq \rho_0^2 \left[1 - \epsilon^2 \left(\frac{b}{B} - \frac{b^2}{B^2} \right) \right]. \quad (\text{A5})$$

The SNR losses will be the smallest when the error on \mathbf{C} is uniform over most of the bandwidth of the signal, as it is the case for narrow-band signals, and obviously when these errors are small where the signal is large compared to the instrumental noise. The worst case scenario is a signal with $b/B = 1/2$, in which case the fractional SNR loss is

$$\sqrt{\frac{\rho_0^2 - \rho^2}{\rho_0^2}} \simeq \frac{\epsilon}{2}. \quad (\text{A6})$$

As similar perturbation analysis can be performed for the parameter estimation problem, by expanding Eqs.(18) and (19) to first order in \mathbf{C}_1 , and then computing $\text{cov } \hat{\lambda}$ as defined in Eq.(16). The inverse of the perturbed Fisher matrix given in Eq.(19) is given by

$$\mathbf{I}^{-1} = \mathbf{I}_0^{-1} + \mathbf{I}_0^{-1} \frac{\partial \tilde{\chi}}{\partial \lambda} \mathbf{C}_0^{-1} \mathbf{C}_1 \mathbf{C}_0^{-1} \frac{\partial \tilde{\chi}^\dagger}{\partial \lambda} \mathbf{I}_0^{-1} + O(\mathbf{C}_1^2), \quad (\text{A7})$$

where \mathbf{I}_0^{-1} is the achievable covariance when the correlation matrix is known exactly ($\mathbf{C}_1 = 0$). Using this and the first order expansion of the inverse of the correlation matrix into Eq.(18) gives four terms that are first order in \mathbf{C}_1 . These four terms can be simplified using the following identities

$$\mathbf{I}_0^{-1} = \mathbf{I}_0^{-1} E \left[\text{Re} \left[\frac{\partial \tilde{\chi}}{\partial \lambda} \mathbf{C}^{-1} (\tilde{\mathbf{x}} - \tilde{\chi})^\dagger \right] \text{Re} \left[\frac{\partial \tilde{\chi}}{\partial \lambda} \mathbf{C}^{-1} (\tilde{\mathbf{x}} - \tilde{\chi})^\dagger \right]^T \right] \mathbf{I}_0^{-1} \quad (\text{A8})$$

$$E[(\mathbf{x} - \boldsymbol{\chi})^\dagger (\mathbf{x} - \boldsymbol{\chi})] = \mathbf{C}_0 \quad (\text{A9})$$

$$E[(\mathbf{x} - \boldsymbol{\chi})^T (\mathbf{x} - \boldsymbol{\chi})] = 0. \quad (\text{A10})$$

The result is that the terms that are first order in \mathbf{C}_1 all cancel, as they did for the SNR. The increase in the covariance of the estimated quantities is therefore at most second order in the errors on the measurement of the correlation matrix.

-
- [1] C. R. Evans, Jr. I. Iben, and L. Smarr, *Astrophys. J.* **323**, 129 (1987) ; D. Hils, P. L. Bender, and R. F. Webbink, *Astrophys. J.* **360**, 75 (1990) ; G. Nelemans, L. R. Yungelson, and S. F. Portegies Zwart, *Astron. Astrophys.* **375**, 890 (2001).
 - [2] LISA Science Requirements document (2002).
 - [3] M. Tinto and J. W. Armstrong, *Phys. Rev. D* **59**, 102003 (1999) ; F. B. Estabrook, M. Tinto, and J. W. Armstrong, *Phys. Rev. D* **62**, 042002 (2000) ; M. Tinto, F. B. Estabrook, and J. W. Armstrong, *Phys. Rev. D* **65**, 082003 (2002) ; M. Tinto, D. A. Shaddock, J. Sylvestre, and J. W. Armstrong, *Phys. Rev. D* **67**, 122003 (2003).
 - [4] J. W. Armstrong, F. B. Estabrook and M. Tinto, *Astrophys. J.* **527**, 814 (1999).
 - [5] M. Tinto, F. B. Estabrook and J. W. Armstrong, "Time-Delay Interferometry and LISA's Sensitivity to Sinusoidal Gravitational Waves", technical document of the LISA project (2002). Available at http://www.srl.caltech.edu/lisa/tdi_wp/LISA_Whitepaper.pdf.
 - [6] D.A. Shaddock, gr-qc/0306125 (2003).
 - [7] N. Cornish and R.W. Hellings, gr-qc/0306096 (2003).
 - [8] D.A. Shaddock, M. Tinto, F.B. Estabrook, and J.W. Armstrong, gr-qc/0307080 (2003).
 - [9] T. A. Prince, M. Tinto, S. L. Larson, and J. W. Armstrong, *Phys. Rev. D* **66**, 122002 (2002).
 - [10] A. Królak and M. Tinto, gr-qc/0302013.
 - [11] M. Tinto, J. W. Armstrong, and F. B. Estabrook, *Phys. Rev. D* **63**, 021101R (2001).
 - [12] C. J. Hogan and P. L. Bender, *Phys. Rev. D* **64**, 062002 (2001).
 - [13] LISA System and Technology Study Report (2000).
 - [14] P. L. Bender, "Suggested Candidate for LISA Error Allocation Budget", unpublished document (2003).
 - [15] J. Sylvestre and M. Tinto, in preparation.
 - [16] W. H. Press et al., *Numerical recipes in C: the art of scientific computing*, Cambridge University Press (1988).
 - [17] P. L. Bender, D. Hils, *Class. Quantum Grav.* **14**, 1439 (1997).